

ELECTROMAGNETIC WAVES SCATTERING AT INTERFACES BETWEEN DIELECTRIC WAVEGUIDES: A REVIEW ON ANALYSIS AND APPLICATIONS

**J. R. García^{1,*}, M. G. Granda², A. F. Gavela¹, S. A. Presa¹,
M. R. Lastra³, and S. F. Fernández¹**

¹Physics Department, University of Oviedo, 33007 Oviedo, Asturias, Spain

²ETH Zurich, Zürich, Switzerland

³Energy Department, University of Oviedo, 33004 Oviedo, Asturias, Spain

Abstract—The scattering properties of dielectric waveguides connected in cascade can be obtained by using the generalized scattering matrix concept, together with the generalized telegraphist equations formalism and the modal matching technique. This review aims to show the potential of periodic structures in dielectric waveguides in order to gain control of light in the design of microwave and photonic devices. The new inverted Π dielectric waveguide is presented. Numerical and experimental results of the complex scattering coefficients were obtained at microwave frequencies. At optical frequencies, results for planar waveguide photonic crystals are included and compared with the numerical values from commercial software. In all cases the agreement was excellent. Electromagnetic and photonic band gaps, photonic windows, optical switching, optical resonant microcavities as well as refractive index optical sensors can be achieved by means of dielectric waveguides in cascade.

1. INTRODUCTION

At microwave frequencies, integrated circuits and devices using dielectric waveguides require transitions from metallic rectangular waveguides to dielectric waveguides, as well as transitions between different dielectric waveguides and dielectric posts [1–8]. At

Received 31 August 2011, Accepted 30 November 2011, Scheduled 9 December 2011

* Corresponding author: José Rodríguez García (jose@uniovi.es).

optical frequencies, periodic dielectric materials offer a great deal of control over the propagation of electromagnetic waves. Periodically segmented optical waveguides, waveguide gratings, photonic bandgap microcavities and waveguide photonic crystals play an important role in applied optics research [9–15]. Several efficient techniques have been reported for the analysis of discontinuities in dielectric waveguides [13–21]. However, these methods have been limited to microwave frequencies and single step discontinuities in dielectric slab waveguides (1-D) [16–21]. Eigenmode expansion methods were presented for analyzing integrated optical devices such as: photonic crystal structures, optical microresonators, vertical-cavity surface-emitting lasers and couplers [13–15]. Apart from these successful proposals, the analysis of single and multiple discontinuities in arbitrary optical waveguides (1-D and 2-D) needs to be both generalized and improved.

In the present paper, the authors provide a review of their experience in the evaluation of the complete electromagnetic scattering caused by multiple abrupt discontinuities in dielectric waveguides with arbitrary sectional geometries and index profile functions. In this work, periodic configurations in rectangular dielectric waveguides at microwave frequencies, as well as in planar integrated optical waveguides are considered. In all cases, the theoretical model encloses the dielectric waveguides by perfectly conducting walls, and the cross section of the resulting guiding system is covered by a grid of pixels so that the refraction index inside each pixel is uniform. This method relies on a new concept of the scattering matrix; consequently, it is called Generalized Scattering Matrix Method (GSMM). In this work, and in order to obtain the Generalized Scattering Matrix (GSM) of any cascaded set of abrupt discontinuities, the Generalized Telegraphist Equations (GTE) formulation [22, 23] and the Modal Matching Technique (MMT) [24, 25] are extended at optical frequencies.

The accuracy and effectiveness of this procedure is analyzed at microwave and optical frequencies. Theoretical and experimental results are obtained for coupled cylindrical dielectric posts, gradual transitions as well as cascaded inverted Π dielectric waveguides, working at microwave frequencies. In all cases, results for the reflection and transmission coefficients (modulus and phase) of the fundamental proper mode are given. Matching between theory and experiment is reported. The possibility of using rectangular metallic waveguides partially filled with coupled dielectric posts and periodic dielectric waveguides, for designing passive devices is confirmed. The method is applied at optical frequencies for analyzing abrupt discontinuities in integrated planar optical waveguides. We demonstrate the possibilities

of designing microwave devices, waveguide photonic crystals as well as optical devices using cascaded dielectric waveguides.

2. THEORY

The complete mathematical algorithm is divided in two steps [22]:

- A) Dielectric waveguides proper modes analysis.
- B) GSM evaluation: single and multiple discontinuities.

2.1. Dielectric Waveguides Proper Modes Analysis

The Modal Matching Technique (MMT) is applied to the analysis of each single discontinuity. Figure 1 is a side view of an abrupt discontinuity between two dielectric waveguides enclosed by perfectly conducting walls separated by a distance $a_{p,ch}$. Subscript p refers to 1-D (slab and planar) dielectric waveguides whereas subscript ch refers to 2-D (image, channel and cylindrical) dielectric waveguides. The application of the MMT requires the evaluation of the dielectric waveguides proper modes. Slab and planar dielectric waveguides (1-D) propagate TE and TM proper modes; however, image and channel dielectric waveguides (2-D) propagate hybrid modes which, in a medium with a diagonal dielectric tensor, can be approximated by E_{pq}^y and E_{pq}^x proper modes [26–32]. The superscript indicates the direction of polarization of the dominant electric field component while the subscript denote the number of maxima, respectively, in the x and y directions. We assume waveguides free from losses, small variations of the index of refraction and propagation along the z axis of the

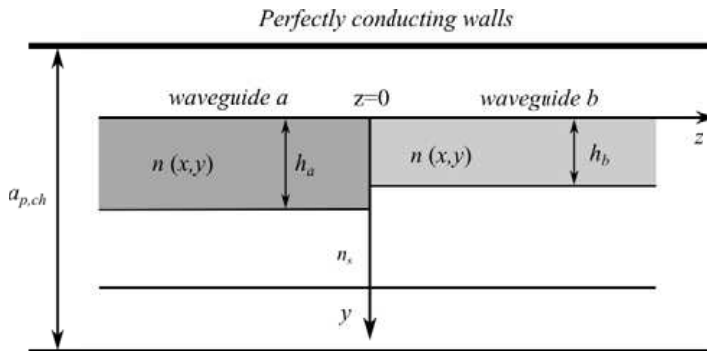


Figure 1. Side view of shielded dielectric waveguides, a and b , in cascade and connected by an abrupt transition.

form $\exp[j(\omega t - \beta z)]$. Under these assumptions, the following two dimensional Helmholtz's equation describes the propagation of the electromagnetic field in terms of the vector electric field \vec{E} , in the waveguide:

$$\nabla_t^2 \vec{E} + [k_0^2 n^2(x, y) - \beta^2] \vec{E} = \vec{0} \quad (1)$$

where k represents the free space wavenumber, β is the phase constant in the propagation direction z and $n(x, y)$ is the refraction index profile for (2-D) dielectric waveguides. This function depends on the dielectric waveguide geometry as well as the fabrication techniques. We assume x and y as the horizontal and vertical coordinates, respectively. For the simplest 1-D and 2-D dielectric waveguides (slab and image dielectric waveguide, respectively), the refraction index functions are:

$$n(x, y) = n = \begin{cases} n_c = 1, & \text{cover (air)} \\ \sqrt{\varepsilon_r}, & \text{core} \end{cases} \quad (2)$$

where $n(x, y) = n(y) = n$ for 1-D dielectric waveguides, and ε_r represents the dielectric constant. For the special case of cylindrical dielectric waveguides and posts, $n(x, y) = n(r)$, and verifies:

$$n(r) = n = \begin{cases} n_c = 1, & \text{cover (air)} \\ f_r, & \text{core} \end{cases} \quad (3)$$

where, usually $f(r) = \sqrt{\varepsilon_r}$.

At optical frequencies, channel optical waveguides show a refraction index profile dependence in the form:

$$n(x, y) = \begin{cases} n_c = 1, & \text{cover (air)} \\ n_s + \Delta n \cdot f(-y/h) \cdot g(x/w), & \text{core} \\ n_s, & \text{substrate} \end{cases} \quad (4)$$

For planar optical waveguides, the refraction index in the core can be written as $n(x, y) = n(y) = n_s + \Delta n \cdot f(-y/h)$.

In Equation (4), n_s is the refractive index of the substrate; Δn refers to the maximum refractive index increment; f and g are the refraction index functions along y and x directions, respectively; h is the diffusion depth, and w represents the width of the channel.

In order to calculate the proper modes, the dielectric waveguides are assumed to be enclosed by perfectly conducting walls. If we are interested in 1-D dielectric waveguides, there is no variation in the x direction, and perfectly conducting parallel plates are used as shielding. For 2-D and cylindrical dielectric waveguides, the transverse variation of the refraction index requires the use of a perfectly conducting shielding with a rectangular cross section.

To simulate the refraction index profile functions, the dielectric waveguide cross section is modeled by a grid or mesh of pixels with

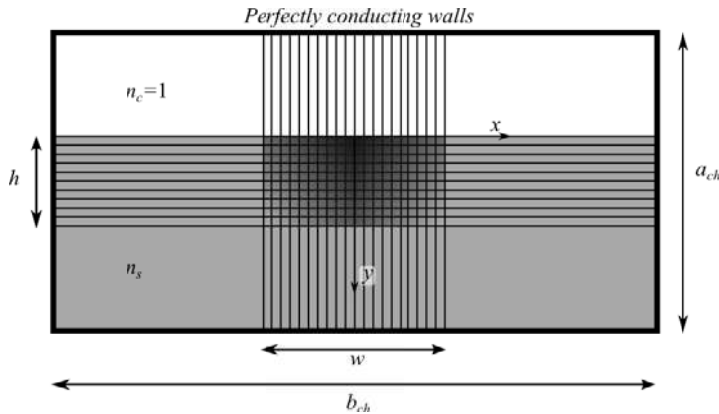


Figure 2. Cross section of a shielded channel optical waveguide modeled by a grid of pixels with different refractive indices.

different refraction index values, as shown in Figure 2 for 2-D dielectric waveguides. The refraction index inside each pixel is uniform and the model allows the use of arbitrarily fine meshes. The importance of using such strategy lies in being able to employ higher mesh refinement when accurate values of the fields are required. Moreover, the model permits the use of variable meshes in zones of particular interest, for example in the channel waveguide core, where refraction index has xy -dependence. The main advantages of enclosing the dielectric waveguides by perfectly conducting boundaries are the following: a) The method does not restrict the dielectric waveguides cross section shape as well as the index profile functions and the frequency band of analysis; consequently, it does not depend on the dielectric waveguides fabrication techniques. b) The algorithm offers functional simplification in the series expansion, it is numerically stable, efficient and accurate. c) It can be applied for analyzing any cascaded set of abrupt discontinuities in arbitrary dielectric waveguides. d) As the method provides all type of proper modes, including evanescent modes solutions, the abrupt discontinuities can be placed as close together as desired; consequently, the study of any dielectric configuration modeled as a cascaded set of abrupt transitions is possible. e) In all cases, for progressively increasing distance between the shielding walls, a distance value is reached at which the proper modes solution matches that of the unshielded dielectric waveguide [1, 33–36]. This situation is achieved when the cross dimensions of the perfectly conducting walls are sufficiently large so that the electromagnetic field perturbation introduced by the shielding can be negligible. This was

demonstrated, theoretically and experimentally, for shielded dielectric waveguides at microwave frequencies [1]. Taking the scalable properties of the electromagnetic wave problems into account, this behavior was investigated and demonstrated theoretically at optical frequencies [33–36].

2.2. GSM Evaluation: Single and Multiple Discontinuities

Regarding Figure 1, we denote as waveguide a and waveguide b the shielded dielectric waveguides located at $z < 0$ and $z > 0$, respectively, of the abrupt discontinuity, at $z = 0$.

In order to apply the MMT and for reducing computational time when calculating the GSM, an adequate number of proper modes which meet at the discontinuity must be selected (M proper modes in waveguide a , and N proper modes in waveguide b). Obviously, we investigate the proper modes which have the highest influence. The criteria used for the selection of the proper modes was the maximization of the coupling integrals between the fundamental proper mode of the waveguide a with all the proper modes solutions in waveguide b , and vice-versa [22]. These coupling integrals appear when applying the MMT, so that the proper modes that maximize them are chosen (Appendix).

Once the selection process is finished, we assume M and N proper modes in waveguides a and b , respectively. Our GSMM formulation implies the evaluation of the contribution of each proper mode to the reflection, both from itself and from the rest of the proper modes in the same waveguide, and to the transmission of all the proper modes of the other waveguide.

Evidently, this effect must be evaluated for each M and N proper mode of waveguides a and b , respectively. In this way, the discontinuity is treated as a device of $M + N$ electromagnetic ports, and each proper mode is taken as an electromagnetic port. Waveguides a and b are considered to be physical ports, labeled as 1 and 2, respectively. Therefore, the GSM of a single discontinuity symbolizes a matrix of electromagnetic ports corresponding to physical ports. This GSM, denoted as $[S]$, can be written as [34]:

$$[S] = \begin{bmatrix} [S_{11}] & [S_{12}] \\ [S_{21}] & [S_{22}] \end{bmatrix} \quad (5)$$

where $[S_{ij}]$ ($i = 1, 2; j = 1, 2$) are submatrices whose complex elements represent the reflection and transmission coefficients between proper modes. Submatrices $[S_{11}]$ and $[S_{21}]$ are obtained when the M proper modes in waveguide a impinge on the discontinuity; in the same way, $[S_{12}]$ and $[S_{22}]$ are calculated taking the N proper modes of waveguide

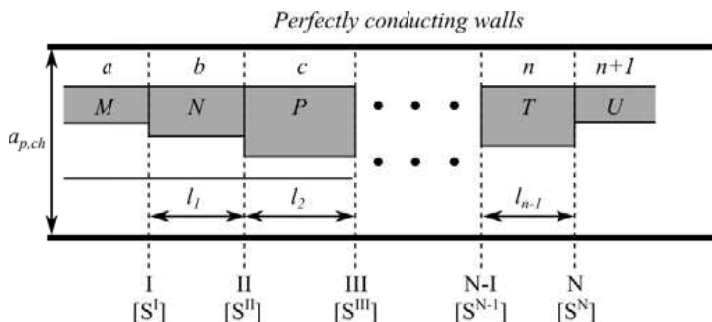


Figure 3. General representation of a cascaded set of N abrupt discontinuities in shielded dielectric waveguides.

b. We denote $[S_{11}]$ and $[S_{22}]$ as submatrices of reflection, whereas $[S_{21}]$ and $[S_{12}]$ are submatrices of transmission.

2.3. GSM of a Cascaded Set of Abrupt Discontinuities

Once the GSM of each abrupt discontinuity has been calculated, we have to determine the total GSM of a cascaded set of abrupt discontinuities. Figure 3 shows a general representation of a cascaded set of N abrupt discontinuities in arbitrary optical dielectric waveguides enclosed by perfectly conducting walls.

We denote the dielectric waveguides using the labels: $a, b, c, \dots, n, n + 1$. The capitals: M, N, P, Q, \dots, T, U represent the number of proper modes to be taken in the successive waveguides, respectively. So, $n + 1$ dielectric waveguides give N cascaded abrupt discontinuities, labeled as: **I, II, III, ..., N - 1, N**. The discontinuities are separated by the dielectric waveguide lengths: $l_1, l_2, l_3, \dots, l_{n-1}$. The successive single GSM's are denoted as: $[S^I], [S^{II}], [S^{III}], \dots, [S^{N-1}], [S^N]$. To determine the total GSM, $[S^T]$, we join the **N** GSM's, two by two and correlatively [34]. Finally, we obtain the total GSM, $[S^T]$, corresponding to the **N** discontinuities. It has the form:

$$[S^T] = \begin{bmatrix} [S_{11}^T(M \times M)] & [S_{12}^T(M \times U)] \\ [S_{21}^T(U \times M)] & [S_{22}^T(U \times U)] \end{bmatrix} \quad (6)$$

where the complex submatrices $[S_{ij}^T]$ ($i = 1, 2; j = 1, 2$) are known.

3. RESULTS

In order to study the scattering characteristics of shielded cylindrical and periodic rectangular dielectric configurations in cascade, we have

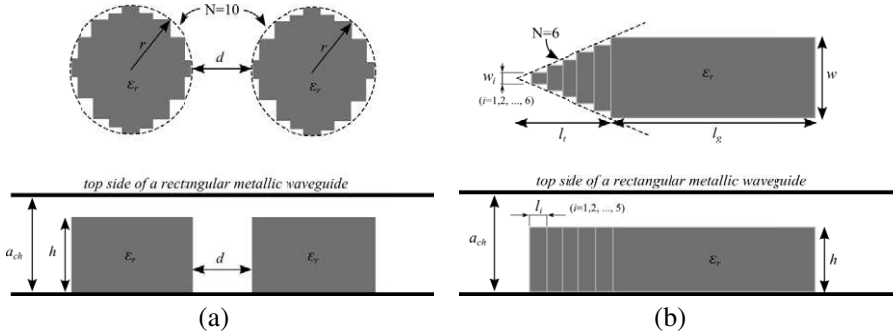


Figure 4. Top and side views of (a) two coupled dielectric posts, and (b) a gradual dielectric transition, enclosed by perfectly conducting boundaries. The modelization as a cascade set of multiple discontinuities is shown.

obtained experimental results which are compared with the theoretical ones. Figure 4 shows two coupled dielectric posts and a dielectric gradual transition, respectively.

The cylindrical posts and the gradual transition were built in polystyrene ($\varepsilon_r = 2.56$), and were fixed to the wider side of the rectangular metallic waveguide with double adhesive tape. The application of this method is not restricted theoretically to symmetrically located dielectrics; however, in order to ensure a good set up, all the dielectrics structures were placed symmetrically with respect to the longitudinal axis, z -axis, of the metallic waveguide typically used in the X -band frequencies ($22.86 \text{ mm} \times 10.16 \text{ mm}$). The circular dielectric waveguides were built in teflon ($\varepsilon_r = 2.1$), and foam ($\varepsilon_r \approx 1$) was used to locate them symmetrically with respect to the longitudinal axis of the rectangular metallic waveguide. In all cases, results of the reflection and transmission coefficients, both moduli and phase, for the fundamental proper mode were measured and compared with the theoretical ones [35]. For this reason, although the complete generalized scattering matrix was calculated, only the first column of the submatrices $[S_{11}^T, S_{21}^T]$ and $[S_{12}^T, S_{22}^T]$ is relevant because we are interested, specifically, in the fundamental proper mode. In order to simplify the results presentation, we denote by R the reflection, S_{11} , and by T the transmission, S_{21} , coefficients.

Figure 5(a) compares the theoretical and experimental results obtained for the reflection coefficient, R , of the fundamental proper mode for two coupled dielectric posts. In this case, two electromagnetic windows appear, at 8.5 GHz and 9.2 GHz. When distance d between the coupled posts is increased, the transparent frequency value

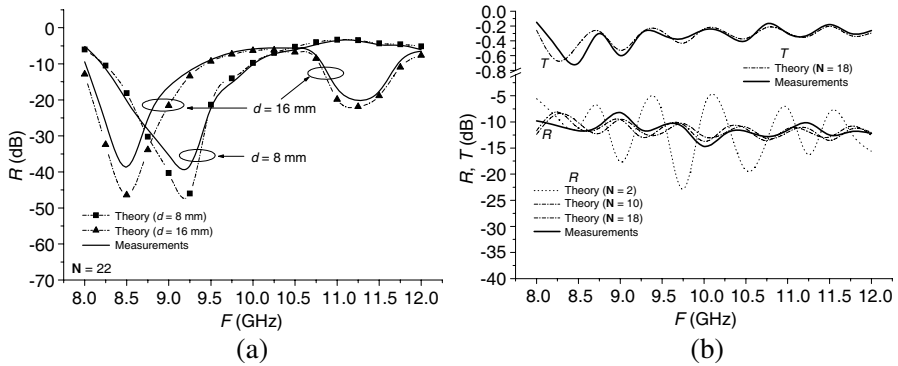


Figure 5. (a) Theoretical and experimental results: moduli of the reflection coefficient, R , of the fundamental proper mode, versus frequency, for the coupled cylindrical dielectric posts in Figure 4(a). Parameters: $h = 8.1$ mm, $r = 8$ mm, $\epsilon_r = 2.56$. (b) Theoretical and experimental results: moduli of the reflection, R , and transmission, T , coefficients, of the fundamental proper mode, versus frequency, for the gradual dielectric transition in Figure 4(b). Parameters: $l_t = 49$ mm, $l_g = 74.5$ mm, $w = 15.02$ mm, $\epsilon_r = 2.56$.

decreases: 9.2 GHz for $d = 8$ mm and 8.5 GHz for $d = 16$ mm. In both cases, the reflection characteristics can be adjusted easily by tuning the desired frequency.

The theoretical results were obtained by using $n + 1 = 21$ dielectric waveguides in cascade ($N = 22$ abrupt discontinuities) in the simulation of each dielectric post. A good agreement is noticed between theory and experiment. The concordance improves when reflection coefficient increases.

The method was applied for analyzing a dielectric gradual transition which connects an empty rectangular metallic waveguide to a shielded image dielectric waveguide. Figure 5(b) shows, for the fundamental proper mode, the theoretical and experimental results obtained for the moduli of the reflection, R , and transmission, T , coefficients. Figure 6 contains the phase results of the gradual transition which was simulated by a set of $N = 18$ abrupt discontinuities in cascade. When N increases, a better simulation of the transition is obtained. In both cases, moduli and phase, the numerical results are very close to the experimental ones when $N = 18$. Additional numerical and experimental results were obtained when shielded cylindrical dielectric waveguides are connected abruptly and gradually. In all cases the concordance was excellent. The possibility of

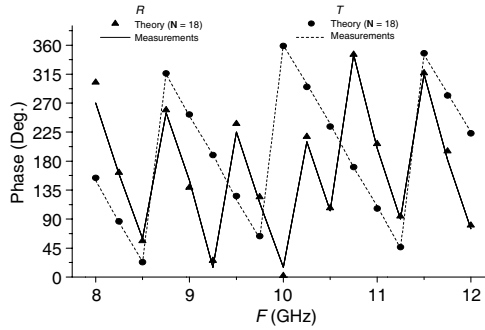


Figure 6. Theoretical and experimental results: phase of the reflection, R , and transmission, T , coefficients, of the fundamental proper mode, versus frequency, for the gradual dielectric transition in Figure 4(b).

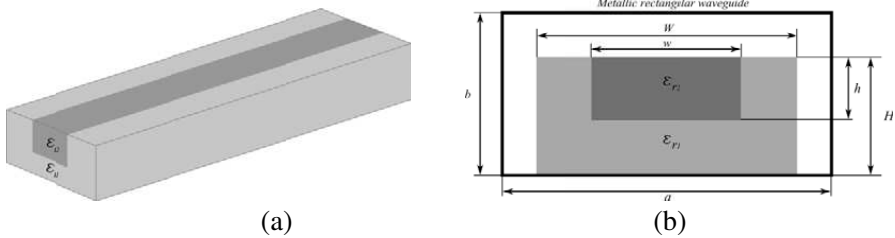


Figure 7. (a) Inverted II dielectric waveguide, and (b) cross section of a shielded inverted II dielectric waveguide. Geometrical and electrical parameters are shown.

designing power dividers and filters using dielectrics with very simple geometry was confirmed.

A new dielectric waveguide is introduced as a good candidate for microwave devices design. We denote it as inverted II dielectric waveguide. The inverted II dielectric waveguide consists of a square dielectric rod (permittivity ϵ_{r1}), with a symmetrical longitudinal channel. The channel may be filled with air or with any other dielectric (permittivity ϵ_{r2}). This dielectric material can be removed from the channel or can be shifted inside it depending on the waveguide application. Figure 7 represents an inverted II dielectric waveguide (a), and the cross section of an inverted II dielectric waveguide inside a metallic rectangular waveguide (b).

We are interested in solving the scattering electromagnetic problem inside metallic rectangular waveguides partially filled with

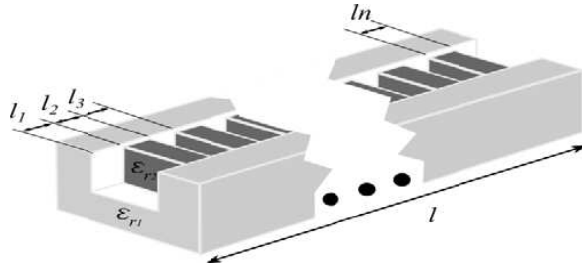


Figure 8. Multiple discontinuities set in inverted II dielectric waveguides connected abruptly.

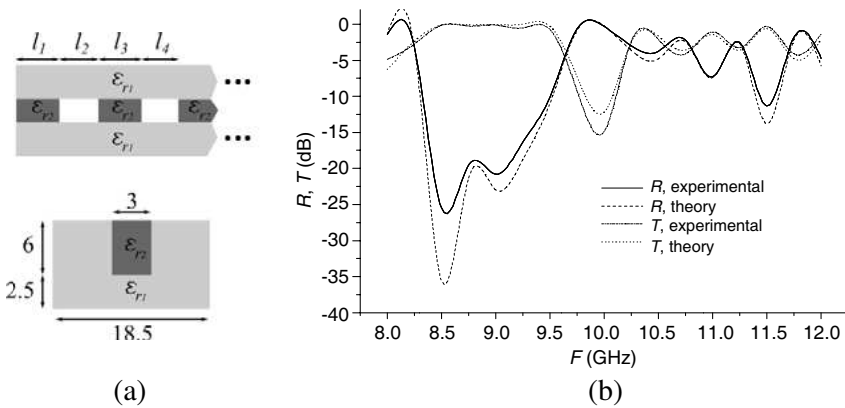


Figure 9. (a) Top view and cross section of a periodical configuration built in inverted II dielectric waveguides connected abruptly. In all cases: $\epsilon_{r1} = 2.1$ (teflon), $\epsilon_{r2} = 10$ (alumina). Dimensions in mm. (b) Theoretical and experimental results. Reflection, R , and transmission, T , coefficients, versus frequency, for the fundamental proper mode. Basic modes number: 30. Proper modes number in all waveguides: 20.

n inverted II dielectric waveguides connected in cascade, as it is shown in Figure 8. As for dielectric posts and transitions, the n inverted II dielectric waveguides were located symmetrically inside the metallic rectangular waveguide ($22.86 \text{ mm} \times 10.16 \text{ mm}$). As an example, Figure 9 shows the calculated transmission and reflection coefficients of a sequence of fifteen cascaded inverted II dielectric waveguides, together with the actual measurement results from the fabricated device.

We have analyzed the behavior of shielded inverted II dielectric waveguides in cascade as Electromagnetic Band Gaps (EBG)

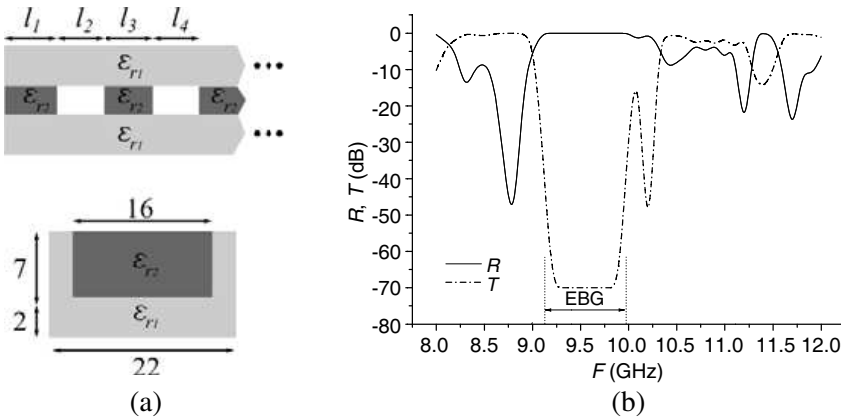


Figure 10. (a) Top view and cross section of a dielectric periodical configuration, in inverted Π dielectric waveguides. In all cases: 23 inverted Π dielectric waveguides in cascade ($\epsilon_{r2} = 1$ (air) in odd order waveguides and $\epsilon_{r2} = 10$ in even order waveguides). Dimensions in mm. (b) Theoretical results. Reflection, R , and transmission, T , coefficients, versus frequency, for the fundamental proper mode. Basic modes number: 20. Proper modes number in all waveguides: 20.

structures. In all cases we have used a sequence of alumina-air-alumina discontinuities in the channel as periodical parameter, as shown in Figure 8. Different periodical configurations were designed and tested. As an example, Figure 10(a) shows a periodic structure and the cross section dimensions. In this case, the physical parameters were as follows: 23 inverted Π dielectric waveguides; conducting walls cross section dimensions (mm); $a = 22.86$, $b = 10.16$; basic modes number: 20; proper modes number: $M = N = P = \dots = 20$; $\epsilon_{r1} = 2.1$ (teflon), $\epsilon_{r2} = 10$ (alumina) in odd order inverted Π dielectric waveguides and $\epsilon_{r2} = 1$ (air) in even order inverted Π dielectric waveguides. Figure 10(b) presents the moduli of the reflection, R , and transmission, T , coefficients for the fundamental proper mode. An EBG, from 9.125 GHz to 10 GHz, was obtained.

The evolution of the Electromagnetic Band Gaps was studied for the case of periodical configurations with one missing alumina block. The sequence of waveguides can now be regarded as a 1-D photonic structure with a defect.

We have demonstrated the influence of the defect position (defect waveguide order) on the EBG bandwidth. Figure 11 shows the reflected, R , and transmitted, T , power surfaces for the fundamental proper mode, as the defect position varies along the channel in the periodical configuration shown in Figure 10(a). In order to make

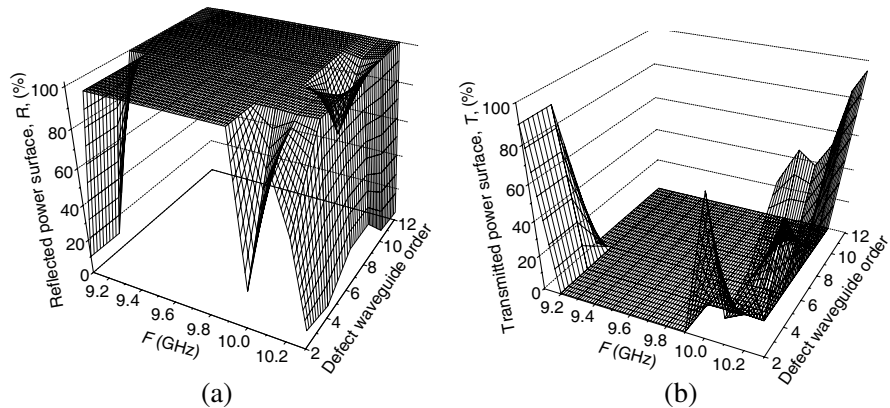


Figure 11. (a) Reflected and (b) transmitted power surfaces for the EBG microwave structure, versus frequency and defect waveguide order, in the frequency band (9.1–10.3) GHz.

the power conservation more evident, we present the moduli of the reflection, R , and transmission coefficients, T , in the power percentages form. If the alumina is removed (a defect is created) in waveguides number 2 or number 4, the EBG is limited to the range between 9.2 GHz and 9.9 GHz. On the other hand, if the defect takes place in waveguide number 6, the EBG spans from 9.2 GHz to 10 GHz. The largest bandwidth of the EBG is given by defect waveguide orders 10 and 12 (9.125 GHz to 10.3 GHz).

Taking into account the scalable properties of the electromagnetic field, the procedure was applied at optical frequencies [35, 36]. Firstly, in order to check the efficiency of the method for finding the proper modes solutions, we have studied extensively its convergence characteristics using all physical parameters of planar and channel optical waveguides. An excellent convergence and good accuracy were noticed for the propagation constant values of the proper modes. The good performance of the method to evaluate optical waveguide proper modes makes possible to use them for analyzing step and gradual transitions in arbitrary optical waveguides.

We have applied the procedure for analyzing periodical structures and waveguide photonic crystals in planar optical waveguides with different lattice constants [36]. The implementation of the pattern waveguide photonic crystal was carried out connecting abruptly 11 planar optical waveguides ($n + 1 = 11$ and $\mathbf{N} = 10$), as shown in Figure 12. The common physical parameters were as follows: conducting walls cross section dimensions (μm): $a_p = 25$, $b_p = 60$; basic modes number: 130; proper modes number: $M = N = P =$

$\dots = 15$; maximum index increments: $\Delta n = 0.01$; diffusion depths (μm): $h = 5$; wavelength: $\lambda = 1 \mu\text{m}$; index profile functions of planar waveguides: exponential; waveguide lengths — lattice constant — (μm): l_i ($i = 2, 3, 4, \dots, 10$) = l . To get the periodic lattice, we use the substrate refractive index, n_s , as lattice periodic parameter, and the waveguide lengths, l , as lattice constant. All optical waveguides are strongly monomode. We assign $n_s = 2.0$ for substrate index of waveguides 1, 3, 5, 7, 9 and 11 (odd order waveguides), while $n_s = 4.0$ is assumed for waveguides 2, 4, 6, 8, 9 and 10 (even order waveguides). In order to show the power conservation, we present the moduli of the reflection R and transmission coefficients T in the power percentages form.

Figure 13 contains the power results in the wavelength interval ($0.93\text{--}1.05$) μm , for the fundamental proper mode, when lattice

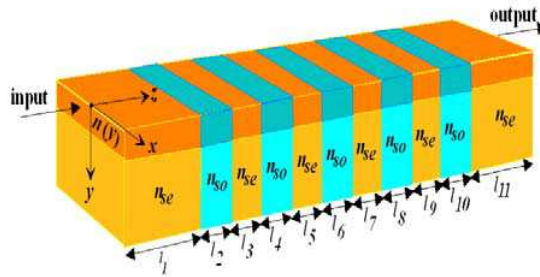


Figure 12. Waveguide photonic crystal in planar optical waveguides.

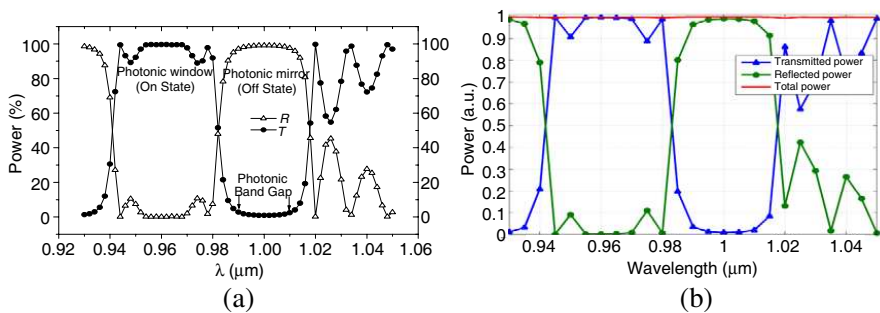


Figure 13. (a) Reflected, R , and transmitted, T , power, versus wavelength, for the fundamental proper mode when lattice constant $l = 1.08 \mu\text{m}$. Periodical structure: ten cascade abrupt discontinuities between planar optical waveguides. (b) Response of the photonic crystal structure calculated with the BEP module of OlympIOs.

constant $l = 1.08 \mu\text{m}$. We show the results obtained with our generalized scattering matrix method in comparison with the results provided by the Bidirectional Eigenmode Propagation (BEP) module of the commercial software OlympIOs. We can notice a transparent behavior for wavelengths in the interval $(0.944\text{--}0.977) \mu\text{m}$. In this wavelength range all the power is transmitted; so, we denote this interval as photonic window (*on state*). However, in the wavelength interval $(0.99\text{--}1.01) \mu\text{m}$ we have an opaque performance and all the power is reflected; so, the periodical structure shows a Photonic Band Gap (PBG) in the interval $(0.99\text{--}1.01) \mu\text{m}$ and it works as a photonic mirror (*off state*) or photonic crystal.

If a local defect is introduced in the PBG structure, an *on state* can be introduced in the gap. The defect can be created by modifying the length or/and the refraction index of the guiding region or the substrate of one of the waveguides. In any case, the introduction of a local defect modifies the optical path length and *on state* can be induced in the PBG structure. In our case, the local defect was engineered modifying the length of waveguide number 6, as Figure 14(a) shows. The performance of the new periodic photonic crystal was extensively studied by the authors [36].

When only one defect is introduced in the waveguide photonic crystal, by changing exclusively the refraction index of the substrate of the central planar waveguide, the device can act as a single channel refraction index optical sensor. On the other hand, when two defects are created, we have a double channel refraction index optical sensor. Naturally, we can introduce the desired number of sensing channels. Figure 14(b) shows the proposed optical sensors with one channel. The refraction index of the specimen filling the channel (defect) is sensed by measuring, simultaneously, the moduli and phase of the reflected and transmitted optical signal. In this way, each measurement is obtained

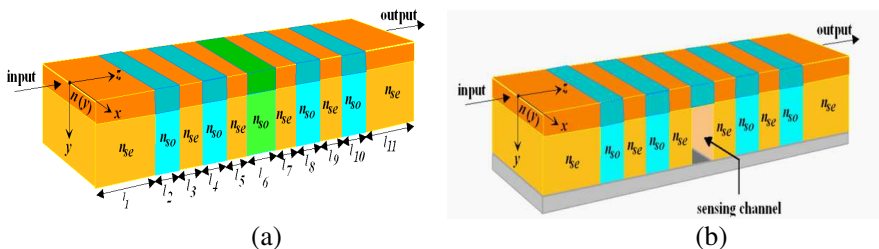


Figure 14. (a) Waveguide photonic crystal with a local defect in waveguide number 6. (b) Refraction index sensor in planar waveguide photonic crystals with one channel.

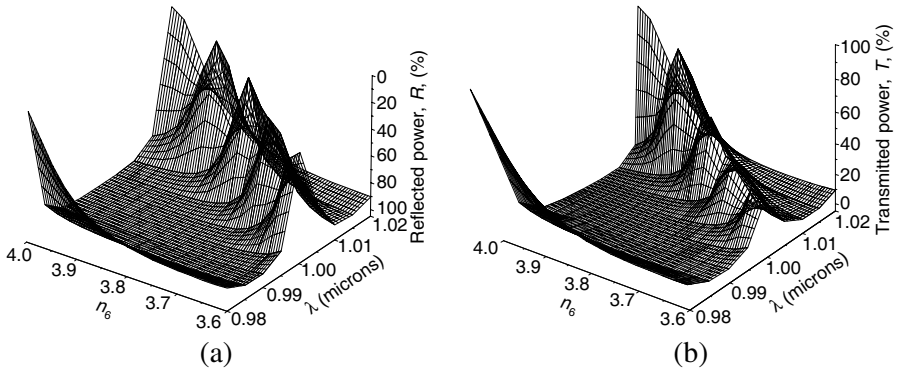


Figure 15. Moduli of (a) reflection and (b) transmission surfaces, versus refraction index and wavelength, for the single channel refraction index optical sensor (vertical axes scaled in an inverted way).

from four magnitudes (two moduli and two phases). Consequently, another important advantage is the accuracy we can obtain in the refraction index evaluation.

In order to show, qualitatively, the first results obtained with the proposed optical sensors, Figures 15(a)–(b) present the moduli of reflection and transmission surfaces, respectively, obtained for the single channel refraction index optical sensor shown in Figure 14(b). The results are given for the E_{pq}^y (TM) fundamental proper mode. In this case the length of the defect, located in the central waveguide, was $l_6 = 1.5147 \mu\text{m}$. To demonstrate the excellent power conservation, in Figures 15(a)–(b), the vertical axis of the reflection and transmission coefficients were scaled in an inverted way. It can be seen that for a given refraction index, the transmission shows a maximum (*on state*) only for a specific wavelength. Besides, the topography of the reflection and transmission power surfaces is almost the same. This behavior justifies the good power conservation, and demonstrates that 95% of the power travels in the TM fundamental proper mode for the analyzed structures. Figure 16 shows the evolution of the minimum reflection values for several refraction indices when $l_6 = 1.5147 \mu\text{m}$. The wavelength position of the minimum provides the refraction index of the specimen to be measured.

The former results suggest that planar waveguide photonic crystals could be useful for refraction index sensors design. Furthermore, refractive index sensors consisting of cascade optical planar waveguide and defects created by microchannels in the substrate may have important advantages when electro-optical materials, such as lithium niobate, are chosen for its manufacture. For example, an

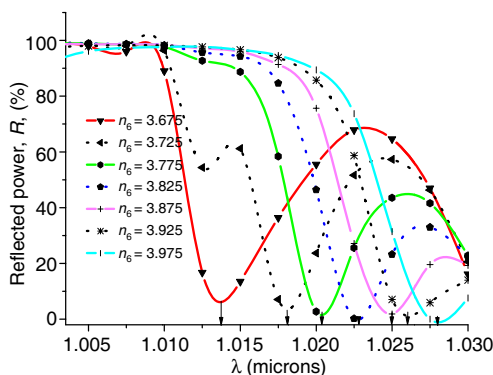


Figure 16. Reflected power, versus wavelength and using the refraction index as parameter, for the single channel refraction index optical sensor when $l_6 = 1.5147 \mu\text{m}$.

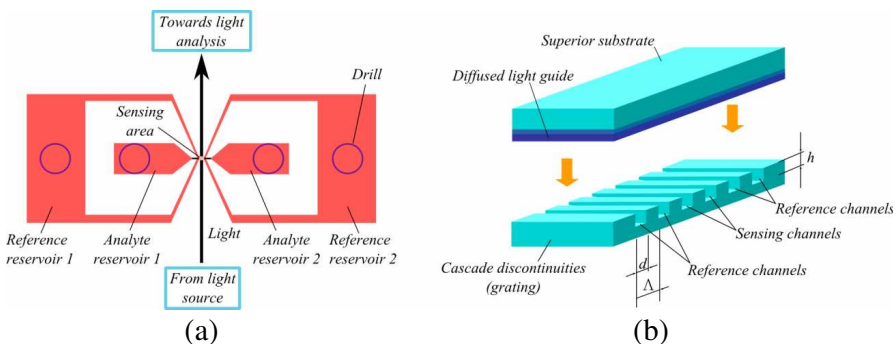


Figure 17. Diagram of the proposed (a) sensing section and (b) fluidic system.

electro-optically driven interferometer at the output of the sensing section can interact with the light in order to measure changes in amplitude and/or phase produced by the analyte. Figure 17(a) is a sketch representing the top view of the proposed sensor.

The diagram includes the sensing area and the reservoirs for analytes and reference fluids. For simplicity, we have drawn only six channels that create discontinuities (defects) in the substrate of the guide: two sensing channels in the center and two reference channels on each side. The parameter Δ represents the lattice constant. The analyte flows through the two central channels (two-channel sensor in this case) while the other two on each side act as a reference. To provide greater flexibility in the measurements, the four reference channels are interconnected and can be filled with another liquid. This

is shown in Figure 17(b), where we can see the sensing area (included in Figure 17(a)) as well as the rest of the proposed fluidic system. To allow the channels fill with the fluid that is desired, the prototype includes two tanks for the analyte and two tanks for reference. Deposits for the analyte are connected to the central channel (sensing), while the two reference tanks are connected to the four remaining channels. It also includes large areas that allow connection of deposits with a fluid system through holes. The new proposed optical sensor is being designed and manufactured by the authors.

4. CONCLUSION

The electromagnetic scattering properties of cascade discontinuities between dielectric waveguides can be obtained by using the generalized scattering matrix (GSM) concept, together with the generalized telegraphist equations (GTE) formulism and the modal matching technique (MMT). This was confirmed by theoretical and experimental evaluation. Commercial Software was used for comparison. The application of the method to cascaded dielectric waveguides has demonstrated the possibility of designing very simple and low cost microwave devices, such as: power dividers, filters, electromagnetic band gaps structures and resonators. At optical frequencies, planar waveguides in cascade conforms another way for light control and photonic devices design. Waveguide photonic crystals, optical switches, narrow transmission optical filters, microresonators as well as refractive index optical sensors can be achieved by means dielectric waveguides in cascade. A new prototype of multichannel refractive optical sensor is proposed in this review.

APPENDIX A.

The electric and magnetic fields, \vec{e}_a and \vec{h}_a , of a normal mode in a metallic rectangular waveguide, “ a ”, partially filled with dielectrics, can be expanded as a series of orthogonal functions which correspond to the electric and magnetic fields of the TE and TM modes of the empty rectangular waveguide:

$$\vec{e}_a(x, y, z) = \sum_i^\infty V_{(i)}(z)\vec{e}_{(i)}(x, y) \quad (\text{A1})$$

$$\vec{h}_a(x, y, z) = \sum_i^\infty I_{(i)}(z)\vec{h}_{(i)}(x, y) \quad (\text{A2})$$

where $V_{(i)}(z)$ and $I_{(i)}(z)$ are the coefficients of the series and represent the equivalent voltages and currents of each normal mode, whereas $\vec{e}_{(i)}(x, y)$ and $\vec{h}_{(i)}(x, y)$ represent the electric and magnetic fields of

TE and TM modes. The subscript (i) refers to TE and TM empty rectangular waveguide modes order.

In order to apply the modal matching technique at the discontinuity between two metallic rectangular waveguides, “ a ” and “ b ”, partially filled with dielectrics, and assuming the two waveguides have the same metallic dimensions, modes TE and TM fulfill the following orthogonal relations:

$$\begin{aligned} \int_a \vec{e}_{a(l)} \times \vec{h}_{a(r)} \cdot \vec{u}_z dx dy &= \int_a \vec{e}_{b(l)} \times \vec{h}_{a(r)} \cdot \vec{u}_z dx dy \\ &= \int_b \vec{e}_{b(r)} \times \vec{h}_{a(l)} \cdot \vec{u}_z dx dy \\ &= \int_b \vec{e}_{b(r)} \times \vec{h}_{b(l)} \cdot \vec{u}_z dx dy = \delta_{lr} \end{aligned} \quad (\text{A3})$$

where \vec{u}_z is the vector of unit magnitude in the z -direction and δ_{lr} is Kroenecker’s delta.

Developing the normal modes of the waveguides “ a ” and “ b ” in their corresponding expressions according to the TE and TM modes, and substituting in (A3), we obtain:

$$\begin{aligned} \int_a \vec{e}_{al} \times \vec{h}_{ar} \cdot \vec{u}_z dx dy &= \int_a \sum_i V_{ak(i)} \vec{e}_{a(i)} \times \sum_j I_{ar(j)} \vec{h}_{a(j)} \cdot \vec{u}_z dx dy \\ &= \sum_i \sum_j V_{al(i)} I_{ar(j)} \int_a \vec{e}_{a(i)} \times \vec{h}_{a(j)} \vec{u}_z \cdot dx dy \\ &= \sum_i V_{al(i)} I_{ar(i)} \end{aligned} \quad (\text{A4})$$

$$\int_a \vec{e}_{bl} \times \vec{h}_{ar} \cdot \vec{u}_z dx dy = \sum_i V_{bl(i)} I_{ar(j)} \quad (\text{A5})$$

$$\int_b \vec{e}_{bl} \times \vec{h}_{ar} \cdot \vec{u}_z dx dy = \sum_i V_{bl(i)} I_{ar(j)} \quad (\text{A6})$$

$$\int_b \vec{e}_{bl} \times \vec{h}_{bl} \cdot \vec{u}_z dx dy = \sum_i V_{bl(i)} I_{br(j)} \quad (\text{A7})$$

where (A5) and (A6) are the coupling integrals of the normal modes of waveguides “ a ” and “ b ”.

ACKNOWLEDGMENT

The authors would like to thank the facilities and the support of Prof. A. Mediavilla, from University of Cantabria, for taking measurements in his lab.

REFERENCES

1. Rodríguez, J. and A. Prieto, "Wide-band directional couplers in dielectric waveguide," *IEEE Trans. Microwave Theory and Techniques*, Vol. 35, 681–687, 1987.
2. Solano, M. A., A. Prieto, et al., "Reduction of losses in dielectric waveguide Y-junctions with wide aperture angles," *Int. Journal of Electronics*, Vol. 63, 741–749, 1987.
3. Strube, J. and F. Arndt, "Rigorous hybrid-mode analysis of the transition from rectangular waveguide to shielded dielectric image guide," *IEEE Trans. Microwave Theory and Techniques*, Vol. 33, 391–401, 1985.
4. Malherbe, J. A. G., J. H. Cloete, et al., "A transition from rectangular to nonradiating dielectric waveguide," *IEEE Trans. Microwave Theory and Techniques*, Vol. 33, 539–543, 1985.
5. Christ, A. and H. L. Hartnagel, "Three-dimensional finite difference method for the analysis of microwave device embedding," *IEEE Trans. Microwave Theory and Techniques*, Vol. 35, 688–696, 1987.
6. Katzier, H., "Streuverhalten elektromagnetischer eellen bei sprunghaften übergängen geschirmter dielektrischer leitungen," *AEÜ*, Vol. 38, 290–296, 1984.
7. Hsu, C.-I. G. and A. Auda Hesham, "Multiple dielectric post in a rectangular waveguide," *IEEE Trans. Microwave Theory and Techniques*, Vol. 34, 883–891, 1986.
8. Leviatan, Y. and G. S. Sheaffer, "Analysis of inductive dielectric posts in rectangular waveguide," *IEEE Trans. Microwave Theory and Techniques*, Vol. 35, 48–59, 1987.
9. Ortega, D., R. M. De La Rue, et al., "Cutoff wavelength of periodically segmented waveguide in Ti:LiNbO₃," *J. Lightwave Technol.*, Vol. 16, No. 2, 284–290, 1998.
10. Moreau, Y., P. Arguel, et al., "Direct printing of gratings on sol-gel layers," *Optical Engineering*, Vol. 37, No. 4, 1130–1135, 1998.
11. Touam, T., M. A. Fardad, M. P. Andrews, and S. I. Najafi, "Sol-gel waveguides with Bragg grating," *Optical Engineering*, Vol. 37, No. 4, 1136–1142, 1998.
12. Foresi, J. S., P. R. Villeneuve, et al., "Photonic-bandgap microcavities in optical waveguides," *Nature*, Vol. 390, 143–145, 1997.
13. Bienstman, P. and R. Baets, "Optical modelling of photonics crystals and VCSELs using eigenmode expansion and perfectly matched layers," *Optical and Quantum Electronics*, Vol. 33, 327–

- 341, 2001.
14. Lohmeyer, M., "Mode expansion modeling of rectangular integrated optical microresonators," *Optical and Quantum Electronics*, Vol. 34, 541–557, 2002.
 15. Gallagher, D. F. G. and T. P. Felici, "Eigenmode expansion methods for simulation of optical propagation in photonics — pros and cons," *Proc. Photonics West*, 4987–4910, 2003.
 16. Brooke, G. H. and M. M. Z. Kharadly, "Step discontinuities on dielectric waveguides," *Electronics Letters*, Vol. 12, 473–475, 1976.
 17. Brooke, G. H. and M. M. Z. Kharadly, "Scattering by abrupt discontinuities on planar dielectric waveguides," *IEEE Trans. Microwave Theory and Techniques*, Vol. 30, 760–770, 1982.
 18. Koshiba, M., K. Ooshi, et al., "Finite-element analysis of the discontinuities in a dielectric slab waveguide bounded by parallel plates," *Electronics Letters*, Vol. 18, 33–34, 1982.
 19. Koshiba, M. and M. Suzuki, "Boundary-element analysis of dielectric slab waveguide discontinuities," *Applied Optics*, Vol. 25, 828–829, 1986.
 20. Weisshaar, A. and V. K. Tripathi, "Modal analysis of step discontinuities in graded-index dielectric slab waveguides," *J. Lightwave Technol.*, Vol. 10, No. 2, 593–602, 1992.
 21. Schmidt, R. and P. Russer, "Modeling of cascade coplanar waveguide discontinuities by the mode-matching approach," *IEEE Trans. Microwave Theory and Techniques*, Vol. 43, No. 12, 2910–2917, 1995.
 22. Rodríguez, J., M. A. Solano, et al., "Characterization of discontinuities in dielectric waveguides using Schelkunoff's method: Application to tapers and transitions," *Int. Journal of Electronics*, Vol. 66, 807–820, 1989.
 23. Rodríguez, J., R. D. Crespo, et al., "Comments on: Verification of generalized telegraphists equations applied to dielectric waveguide problems," *Applied Optics*, Vol. 33, No. 3, 356–357, 1994.
 24. Wexler, A., "Solution of waveguide discontinuities by modal analysis," *IEEE Trans. Microwave Theory and Techniques*, Vol. 15, No. 9, 508–517, 1967.
 25. James, G. L., "On the problem of applying mode-matching techniques in analyzing conical waveguide discontinuities," *IEEE Trans. Microwave Theory and Techniques*, Vol. 31, No. 9, 718–723, 1983.
 26. Marcatili, E. A. J., "Dielectric rectangular waveguide and directional couplers for integrated optics," *Bell System Technical*

- Journal*, Vol. 48, 2071–2102, 1969.
27. Knox, R. M. and P. P. Toullos, “Rectangular dielectric image lines for millimeter integrated circuits,” *1970 Wescon Conference*, 1970.
 28. Knox, R. M. and P. P. Toullos, “Integrated circuits for the millimeter through optical frequency range,” *Symposium on Submillimeter Waves*, 497–516, 1970.
 29. Steinberg, R. A. and T. G. Giallorenzi, “Modal fields of anisotropic channel waveguides,” *J. Opt. Soc. Am.*, Vol. 67, No. 4, 523–533, 1977.
 30. Solbach, K. and I. Wolff, “The electromagnetics fields and phase constants of dielectric image lines,” *IEEE Trans. Microwave Theory and Techniques*, Vol. 26, 266–274, 1978.
 31. Suhara, T., Y. Handa, et al., “Analysis of optical channel waveguides and directional couplers with graded-index profile,” *J. Opt. Soc. Am.*, Vol. 6, 807–815, 1979.
 32. Strake, E., G. P. Bava, et al., “Guided modes of Ti:LiNbO₃ channel waveguides: A novel quasi-analytical technique in comparison with the scalar finite-element method,” *J. Lightwave Technol.*, Vol. 6, No. 6, 1126–1135, 1988.
 33. Crespo, R. D., “Coupled mode theory application for analyzing the electromagnetic propagation characteristics in optical waveguides with arbitrary index profile,” Doctoral Thesis, University of Oviedo, Spain, 1997.
 34. Rodríguez, J., O. Hidalgo, et al., “Photonic devices in waveguide periodical structures: Generalized analysis of multiple discontinuities,” *Optical Engineering*, Vol. 41, No. 8, 1947–1956, 2002.
 35. Rodríguez, J., O. Hidalgo, et al., “Photonic band gaps and photonic windows in cascaded optical waveguides: A complete analysis of the electromagnetic scattering properties,” *Physica Status Solidi (C)*, Vol. 0, No. 5, 1408–1411, 2003.
 36. Rodríguez, J., M. G. Granda, et al., “Planar waveguide photonic crystals as an alternative for refractive index optical sensors design: Theoretical evaluation,” *Journal of Modern Optics*, Vol. 56, No. 7, 927–935, 2009.